First-principles calculation of magnetic x-ray dichroism in Fe and Co multilayers

G. Y. Guo
SERC Daresbury Laboratory, Warrington WA4 4AD, United Kingdom

H. Ebert
Institute for Physical Chemistry, University of München, 80033 München, Germany

W. M. Temmerman and P. J. Durham
SERC Daresbury Laboratory, Warrington WA4 4AD, United Kingdom

(Received 30 November 1993)

A relativistic, spin-polarized band theory of magnetic x-ray dichroism (MXD) in solids is briefly described. Calculated circular and linear dichroic x-ray absorptions at the $L_{2,3}$ edges from bulk Fe and Co as well as from their multilayers [Fe_2Cu_6 (001), $FeAg_5$ (001), $Co_2Pd(Pt)_4$ (111), and Co_2Cu_6 (001)] are presented. Large circular MXD is predicted in both the bulks and the multilayers while linear MXD due to magnetocrystalline anisotropy is found to be small (within 1%). Nevertheless, linear MXD due to a photon polarization change is about 3–8 %. The orbital magnetization sum rule of B. T. Thole *et al.*, [Phys. Rev. Lett. **68**, 1943 (1992)] is found to give orbital magnetic moments too small by about 20–35 %. We note that for each ion species, there is a simple linear relationship between the integrated circular MXD signal and the orbital magnetic moment, and we propose that one uses this linear relationship to measure the orbital magnetic moment of an ion in magnetic solids. The recently proposed spin magnetization sum rule [P. Carra *et al.*, Phys. Rev. Lett. **70**, 694 (1993)] is found to give rather accurate spin magnetic moments for the Co systems (errors within 15%). However, it does not hold qualitatively for highly anisotropic systems such as Fe multilayers.

I. INTRODUCTION

The development of tunable, intense, polarized synchrotron radiation sources has stimulated considerable interest in using x rays to study magnetism in solids in the past years.[1–3] Among the more promising experiments are circular and linear magnetic x-ray dichroism.[2,3] For example, Schütz *et al.*[2] demonstrated that circular magnetic x-ray dichroism (CMXD), measured as the difference in the absorption rate for left and right circularly polarized incident x rays, provide useful information on the spin-dependent, local density of states. Thole *et al.*,[4] on the other hand, showed that, within their atomic multiplet theory, local orbital magnetic moment is related to the integral of the CMXD signal over a given absorption edge by a sum rule. More recently, Kuiper *et al.*[5] showed that in conjunction with theoretical calculations, the orientation of local magnetic moment may be determined by large linear magnetic x-ray dichroism (LMXD).

It is well known that magnetic dichroism is due to the *simultaneous* occurrence of relativistic effects (mainly spin-orbit coupling) and spin polarization in magnetic solids.[6] Therefore, theories of magnetic dichroism should be formulated within a framework of relativistic theory such as relativistic spin-density-function theory.[7] Recently, a description of CMXD, based on a relativistic, spin-polarized multiple-scattering theory,[8] has been developed,[9] and applied to, e.g., bulk Fe,[9] and Fe and Co alloys.[10] The agreement between the theory and experiments was found to be satisfactory. However, the multiple-scattering technique is computationally very demanding, and for complex systems such as magnetic multilayers, calculations of this kind are very formidable. Thus, for magnetic multilayers, a theory based on faster band-theoretical methods is desirable. The computationally efficient linear muffin-tin orbital (LMTO) method[11] has recently been extended to treat relativistic effects and spin polarization on an equal footing.[12] This spin-polarized, relativistic LMTO (SPR-LMTO) method has also been made a self-consistent technique and used to study the magnetocrystalline anisotropy of bulk Fe and Ni (Ref. 13) as well as Fe monolayers and multilayers.[14] In this paper, we briefly describe a band theory of MXD based on the SPR-LMTO method. We present calculated circular and linear dichroic x-ray spectra at the $L_{2,3}$ edge for bulk Fe and Co as well as for their multilayers [Fe_2Cu_6 (001), $FeAg_5$ (001), $Co_2Pd(Pt)_4$ (111), and Co_2Cu_6 (001)].

The organization of the rest of this paper is as follows. In Sec. II, we briefly describe a theory of MXD based on our SPR-LMTO method. In Sec. III, we report calculated spin and orbital magnetic moments. In Sec. IV, we present calculated CMXD and compare them with experiments. In Sec. V, we report calculated LMXD. In Sec. VI, we analyze the recently proposed orbital and spin magnetization sum rules[4,15] in terms of our band-theoretical results. Finally, a summary is given in Sec. VII.

II. THEORY OF POLARIZED X-RAY ABSORPTION

The x-ray absorption coefficient μ of a solid is proportional to the sum of the absorption rates W for various in-

itial core states Λ. Within the standard single-particle theory, the absorption rate for incident x ray of polarization λ and photon energy $\hbar\omega$ by atomic species t, is given by the golden rule, i.e.,

$$W^{\lambda}_{\Lambda}(\omega)=\sum_{j\mathbf{k}}|M^{\lambda}_{\Lambda,j\mathbf{k}}|^2\delta(E_{j\mathbf{k}}-E_{\Lambda}-\hbar\omega)\delta(E_{j\mathbf{k}}-E_f)$$
$$=\sum_{j\mathbf{k}}|\langle\Psi_{j\mathbf{k}}|\Pi_{\lambda}|\Phi^{t}_{\Lambda}\rangle|^2$$
$$\times\delta(E_{j\mathbf{k}}-E_{\Lambda}-\hbar\omega)\delta(E_{j\mathbf{k}}-E_f)\ , \qquad (2.1)$$

where Φ^{t}_{Λ} is the initial core state, $\Psi_{j\mathbf{k}}$ is the final unoccupied (band) state, E_f is the Fermi energy, and Π_{λ} is the electron-photon interaction operator. Hence, the λ polarized x-ray absorption coefficient $\mu^{\lambda}_{\alpha}(\omega)$ for a given absorption edge (α) is (ignoring a constant)

$$\mu^{\lambda}_{\alpha}(\omega)=\sum_{\Lambda}^{\alpha\text{-shell}}W^{\lambda}_{\Lambda}(\hbar\omega)\ . \qquad (2.2)$$

Since MXD is a relativistic effect, we worked within the framework of the SPR-LMTO method.[12] In the relativistic approach, the dipole electron-photon interaction operator is

$$\Pi_{\lambda}=-e\alpha\cdot\mathbf{a}_{\lambda} \qquad (2.3)$$

where $\alpha=\begin{pmatrix}0 & \sigma\\ \sigma & 0\end{pmatrix}$ is the Dirac matrix vector and $\mathbf{a}_{\lambda}$ is the λ polarization unit vector of the photon potential vector $[a_{\pm}=1/\sqrt{2}(1,\pm i,0),a_z=(0,0,1)]$. (Here $+/-$ denotes, respectively, left and right circular photon polarizations with respect to the magnetization direction in the solid.) Both the initial state wave functions Φ^{t}_{Λ} and final state wave functions $\Psi_{j\mathbf{k}}$ were the Dirac four spinors. Φ^{t}_{Λ} were the core-level solutions to the spin-polarized Dirac equation,[16]

$$\Phi^{t}_{\Lambda}(\mathbf{r})=\begin{bmatrix}g^{c}_{\Lambda}(r)\chi_{\Lambda}(\hat{r})+g^{c}_{\bar{\Lambda}}(r)\chi_{\bar{\Lambda}}(\hat{r})\\ if^{c}_{\Lambda}(r)\chi_{-\Lambda}(\hat{r})+if^{c}_{\bar{\Lambda}}(r)\chi_{-\bar{\Lambda}}(\hat{r})\end{bmatrix}\ , \qquad (2.4)$$

where

$$\Lambda=(\kappa,\mu)\ ,\quad -\Lambda=(-\kappa,\mu)\ ,\quad \bar{\Lambda}=(-\kappa-1,\mu)\ ,$$

and $\chi_{\Lambda}(\hat{r})$ is the well known two-component spin angular function.[17] $\Psi_{j\mathbf{k}}$ were the SPR-LMTO band states,[12]

$$\Psi_{j\mathbf{k}}=\sum_{q\Lambda'}[A^{j\mathbf{k}}_{q\Lambda'}\Phi^{q}_{\Lambda'}+B^{j\mathbf{k}}_{q\Lambda'}\dot{\Phi}^{q}_{\Lambda'}] \qquad (2.5)$$

where q is the index for atoms in the primitive cell, over-dot denotes energy derivative and

$$\Phi_{\Lambda'}(\mathbf{r})=\begin{bmatrix}g_{\Lambda'}(r)\chi_{\Lambda'}(\hat{r})+g_{\bar{\Lambda}'}(r)\chi_{\bar{\Lambda}}(\hat{r})\\ if_{\Lambda'}(r)\chi_{-\Lambda'}(\hat{r})+if_{\bar{\Lambda}'}(r)\chi_{-\bar{\Lambda}}(\hat{r})\end{bmatrix}$$

and analogously for $\dot{\Phi}_{\Lambda'}(\mathbf{r})$ with g and f replaced by $\dot{g}$ and $\dot{f}$. The expansion coefficients $A^{j\mathbf{k}}_{q\Lambda}$ and $B^{j\mathbf{k}}_{q\Lambda}$ for band index j and wave vector $\mathbf{k}$ are determined by the corresponding eigenvector.[11,12] Note that in the spin-polarized case, κ is no longer a good quantum number because of the coupling between (κ,μ) and $(-\kappa-1,\mu)$ channels.[8,12,16] Thus, $\Lambda=(\kappa,\mu)$ refers only to the dominant character of the state Λ wave function near the nucleus.

Therefore, the transition-matrix element $M^{\lambda}_{\Lambda,j\mathbf{k}}$, is given by

$$M^{\lambda}_{\Lambda,j\mathbf{k}}=\left\langle\sum_{q\Lambda'}[A^{j\mathbf{k}}_{q\Lambda'}\Phi^{q}_{\Lambda'}+B^{j\mathbf{k}}_{q\Lambda'}\dot{\Phi}^{q}_{\Lambda'}]|\Pi_{\lambda}|\Phi^{t}_{\Lambda}\right\rangle$$
$$=\sum_{q\Lambda'}[A^{j\mathbf{k}}_{q\Lambda'}\langle\Phi^{q}_{\Lambda'}|\Pi_{\lambda}|\Phi^{t}_{\Lambda}\rangle$$
$$+B^{j\mathbf{k}}_{q\Lambda'}\langle\dot{\Phi}^{q}_{\Lambda'}|\Pi_{\lambda}|\Phi^{t}_{\Lambda}\rangle]\delta_{q,t}\ . \qquad (2.6)$$

The $\mathbf{k}$-independent part of the transition-matrix element $\langle\Phi^{q}_{\Lambda'}|\Pi_{\lambda}|\Phi^{t}_{\Lambda}\rangle$ is then given by

$$\langle\Phi_{\Lambda'}|\Pi_{\lambda}|\Phi_{\Lambda}=\left\langle\begin{matrix}g_{\Lambda'}\chi_{\Lambda'}\\ if_{\Lambda'}\chi_{-\Lambda'}\end{matrix}\middle|\Pi_{\lambda}\middle|\begin{matrix}g^{c}_{\Lambda}\chi_{\Lambda}\\ if^{c}_{\Lambda}\chi_{-\Lambda}\end{matrix}\right\rangle$$
$$+\left\langle\begin{matrix}g_{\bar{\Lambda}'}\chi_{\bar{\Lambda}}\\ if_{\bar{\Lambda}'}\chi_{-\bar{\Lambda}}\end{matrix}\middle|\Pi_{\lambda}\middle|\begin{matrix}g^{c}_{\Lambda}\chi_{\Lambda}\\ if^{c}_{\Lambda}\chi_{-\Lambda}\end{matrix}\right\rangle$$
$$+\left\langle\begin{matrix}g_{\Lambda'}\chi_{\Lambda'}\\ if_{\Lambda'}\chi_{-\Lambda'}\end{matrix}\middle|\Pi_{\lambda}\middle|\begin{matrix}g^{c}_{\bar{\Lambda}}\chi_{\bar{\Lambda}}\\ if^{c}_{\bar{\Lambda}}\chi_{-\bar{\Lambda}}\end{matrix}\right\rangle$$
$$+\left\langle\begin{matrix}g_{\bar{\Lambda}'}\chi_{\bar{\Lambda}}\\ if_{\bar{\Lambda}'}\chi_{-\bar{\Lambda}}\end{matrix}\middle|\Pi_{\lambda}\middle|\begin{matrix}g^{c}_{\bar{\Lambda}}\chi_{\bar{\Lambda}}\\ if^{c}_{\bar{\Lambda}}\chi_{-\bar{\Lambda}}\end{matrix}\right\rangle \qquad (2.7)$$

with a similar formula for $\langle\dot{\Phi}^{q}_{\Lambda'}|\Pi_{\lambda}|\Phi^{t}_{\Lambda}\rangle$. Furthermore, the terms in the above equation can be written as radial and angular parts. For example,

$$\left\langle\begin{matrix}g_{\Lambda'}\chi_{\Lambda'}\\ if_{\Lambda'}\chi_{-\Lambda'}\end{matrix}\middle|\Pi_{\lambda}\middle|\begin{matrix}g^{c}_{\Lambda}\chi_{\Lambda}\\ if^{c}_{\Lambda}\chi_{-\Lambda}\end{matrix}\right\rangle$$
$$=-ie[R^{1}_{\Lambda',\Lambda}A^{\lambda}_{\Lambda',-\Lambda}-R^{2}_{\Lambda',\Lambda}A^{\lambda}_{-\Lambda',\Lambda}] \qquad (2.8)$$

where

$$R^{1}_{\Lambda',\Lambda}=\int r^2dr\,g_{\Lambda'}(r)f^{c}_{\Lambda}(r)\ ,\quad R^{2}_{\Lambda',\Lambda}=\int r^2dr\,f_{\Lambda'}(r)g^{c}_{\Lambda}(r)\ ,$$

$$A^{\lambda}_{\Lambda',-\Lambda}=\int d\Omega\,\chi^{\dagger}_{\Lambda'}\sigma\cdot a_{\lambda}\chi_{-\Lambda}\ ,\quad A^{\lambda}_{-\Lambda',\Lambda}=\int d\Omega\,\chi^{\dagger}_{-\Lambda'}\sigma\cdot a_{\lambda}\chi_{\Lambda}\ .$$

Similar formulas exist for the other three terms. The dipole selection rules are determined by the angular integrals $A^{\lambda}_{\Lambda',-\Lambda}$ and $A^{\lambda}_{-\Lambda',\Lambda}$. For left and right circularly polarized x rays $a_{\pm}=(1/\sqrt{2})(1,\pm i,0)$,

$$A^{\pm}_{\Lambda',-\Lambda}=\langle\chi_{\Lambda'}|\sigma_x\pm i\sigma_y|\chi_{-\Lambda}\rangle$$
$$=\frac{2}{\sqrt{2}}\begin{Bmatrix} C(l'\tfrac{1}{2}j';\mu;-\tfrac{1}{2},\tfrac{1}{2})C(\bar{l}\tfrac{1}{2}j;\mu+\tfrac{1}{2},-\tfrac{1}{2})\delta_{l'\bar{l}}\delta_{\mu'-\mu,+1} \\ C(l'\tfrac{1}{2}j';\mu'+\tfrac{1}{2},-\tfrac{1}{2})C(\bar{l}\tfrac{1}{2}j;\mu-\tfrac{1}{2},+\tfrac{1}{2})\delta_{l'\bar{l}}\delta_{\mu'-\mu,-1}\end{Bmatrix}, \quad (2.9a)$$

$$A^{\pm}_{-\Lambda',\Lambda}=\langle\chi_{-\Lambda'}|\sigma_x\pm i\sigma_y|\chi_{\Lambda}\rangle$$
$$=\frac{2}{\sqrt{2}}\begin{Bmatrix} C(\bar{l}'\tfrac{1}{2}j';\mu'-\tfrac{1}{2},\tfrac{1}{2})C(l\tfrac{1}{2}j;\mu+\tfrac{1}{2},-\tfrac{1}{2})\delta_{\bar{l}'l}\delta_{\mu'-\mu,+1} \\ C(\bar{l}'\tfrac{1}{2}j';\mu'+\tfrac{1}{2},-\tfrac{1}{2})C(l\tfrac{1}{2}j;\mu-\tfrac{1}{2},+\tfrac{1}{2})\delta_{\bar{l}'l}\delta_{\mu'-\mu,-1}\end{Bmatrix}, \quad (2.9b)$$

where $\bar{l}=l-s_\kappa$, $s_\kappa=\pm1(\kappa\gtrless0)$. Thus, the selection rules are $\mu'=\mu\pm1(\lambda=\pm)$, $l'=l\pm1$. The other six angular integrals result in the same selection rules. It is the different selection rules for left and right circular polarizations plus the splittings in the conduction bands caused by the spin-polarization and spin-orbit coupling (relativistic effect) which give rise to the circular magnetic x-ray dichroism. Similarly, for z-polarized photons $a_z=(0,0,1)$,

$$A^{z}_{\Lambda',-\Lambda}=\langle\chi_{\Lambda'}|\sigma_z|\chi_{-\Lambda}\rangle$$
$$=[C(l'\tfrac{1}{2}j';\mu'-\tfrac{1}{2},\tfrac{1}{2})C(\bar{l}\tfrac{1}{2}j;\mu-\tfrac{1}{2},\tfrac{1}{2})$$
$$-C(l'\tfrac{1}{2}j';\mu'+\tfrac{1}{2},-\tfrac{1}{2})$$
$$\times C(\bar{l}\tfrac{1}{2}j;\mu+\tfrac{1}{2},-\tfrac{1}{2})]\delta_{l'\bar{l}}\delta_{\mu',\mu}, \quad (2.10a)$$

$$A^{z}_{-\Lambda',\Lambda}=\langle\chi_{-\Lambda'}|\sigma_z|\chi_{\Lambda}\rangle$$
$$=[C(\bar{l}'\tfrac{1}{2}j';\mu'-\tfrac{1}{2},\tfrac{1}{2})C(\bar{l}\tfrac{1}{2}j;\mu-\tfrac{1}{2},\tfrac{1}{2})$$
$$-C(\bar{l}'\tfrac{1}{2}j';\mu'+\tfrac{1}{2},-\tfrac{1}{2})$$
$$\times C(\bar{l}\tfrac{1}{2}j;\mu+\tfrac{1}{2},-\tfrac{1}{2})]\delta_{\bar{l}'l}\delta_{\mu',\mu}. \quad (2.10b)$$

Therefore, the selection rules for z polarization are $\mu'=\mu(\lambda=z)$, $l'=l\pm1$. Again, the other six angular integrals result in the same selection rules. The selection rules for x- and y-polarized photons $[a_x=(1,0,0)=1/\sqrt{2}(a_+ +a_-), a_y=1/i\sqrt{2}(a_+ -a_-)]$ are mixtures of the selection rules for left and right circularly polarized photons.

Calculation of $\mu^{\lambda}_{\alpha}(\omega)$ is then the same as calculation of the weighted (or angular momentum decomposed) density of states. Here, the weighting function is $|M^2_{\Lambda,j\mathbf{k}}|^2$. In the present calculations, the tetrahedron technique[18] was used for the Brillouin-zone integration. More details may be found in a forthcoming paper.[19]

III. ELECTRONIC AND MAGNETIC PROPERTIES

In this paper, we study Fe_2Cu_6 (001) and Co_2Pd_4 (111) multilayers because the experimental CMXD from these systems has been reported recently.[20,21] For comparison, we also study bulk bcc Fe and hcp Co as well as $FeAg_5$ (001), Co_2Pt_4 (111), and Co_2Cu_6 (001) multilayers. We first performed self-consistent electronic-structure calculations using the SPR-LMTO method.

We used the experimental lattice constants for bcc Fe ($a=2.87$ Å) and hcp Co ($a=2.51$ Å and $c/a=1.622$). There is no experimental structural data for most of the multilayers considered here. First-principles determination of the minimum energy structures is beyond the scope of this paper. Therefore, we assumed that Fe_2Cu_6 (001) adopts the ideal fcc Cu crystal structure and the multilayer is equivalent to the fcc Cu with every seventh and eighth Cu layer in the [001] direction being replaced by Fe monolayers. The resultant system has a tetragonal symmetry with $a=a^{\mathrm{Cu}}_{\mathrm{fcc}}/\sqrt{2}=2.56$ Å and $c/a=4\sqrt{2}$. For $FeAg_5$ (001) (Ref. 14) and Co_2Cu_6 (001), we also assumed that they adopt the ideal fcc Ag (Cu) structures with lattice constants of 2.89 and 2.56 Å, respectively. We also assumed that the lattice constant (a) of the hexagonal basal planes in $Co_2Pd(Pt)_4$ (111) is determined by bulk fcc Pd (Pt), i.e., $a=a^{\mathrm{Pd(Pt)}}_{\mathrm{fcc}}/\sqrt{2}=2.75$ (2.77) Å. The lattice constant normal to the basal plane (c) is given by $c=3d_{\text{Pd-Pd (Pt-Pt)}}+2d_{\text{Pd(Pt)-Co}}+d_{\text{Co-Co}}$. We took interlayer spacings $d_{\text{Pd-Pd (Pt-Pt)}}$ of 2.25 (2.26) Å and $d_{\text{Co-Co}}$ of 2.0 Å from bulk fcc Pd (Pt) and Co, respectively. The interlayer spacing $d_{\text{Pd(Pt)-Co}}$ of 2.12 (2.13) Å is an average of $d_{\text{Pd-Pd (Pt-Pt)}}$ and $d_{\text{Co-Co}}$. The resultant supercell $Co_2Pd(Pt)_4$ (111) has a trigonal symmetry.

In all self-consistent calculations, the basis functions were s, p, and d LMTO's. The number of $\mathbf{k}$ points over the irreducible wedge of the Brillouin zone (BZ) used, is 420 (over $\frac{3}{48}$ BZ) for bcc, 396 (over $\frac{1}{24}$ BZ) for hcp Co, 364 (over $\frac{1}{16}$ BZ) for $FeAg_5$ (001) and $Fe(Co)_2Cu_6$ (001), and 388 (over $\frac{1}{12}$ BZ) for $Co_2Pd(Pt)_4$ (111). The usual local exchange-correlation potential of von Barth and Hedin was used.[22] The core charge densities were "frozen." The magnetization direction is set normal to the basal plane or z axis (001). The results of these calculations are summarized in Table I.

As expected, the magnetic moments especially the orbital magnetic moment, of Fe (Co) atom in all the multilayers except Co_2Cu_6 are considerably larger than in the bulk Fe (Co). Interestingly, the induced magnetic moments on the substrate Cu (Ag) next to the magnetic Fe (Co) monolayers are very small in comparison with that on the substrate Pd (Pt) (see Table I). In fact, magnetic moments in the Cu (Ag) monolayers below the top Cu (Ag) monolayer are effectively zero and thus not listed in

TABLE I. Calculated magnetic properties of $Fe(Co)_2Cu_6$ (001), Fe_1Ag_5 (001) and $Co_2Pd(Pt)_4$ (111) multilayers as well as bulk bcc Fe and hcp Cu. m_s (m_o) is the spin (orbital) magnetic moment and m the total magnetic moment. n_e is the total electron charge in an atomic sphere. R_{WS} is the atomic sphere radius used. Cu(Pd,Ag or Pt)n denotes Cu(Pd,Ag or Pt) in the nth layer below the interface Fe (Co) layer.

System	Atom	R_{WS} (A)	m_s (μ_B/atom)	m_o (μ_B/atom)	m (μ_B/atom)	n_e
bcc Fe		1.409	2.200	0.043	2.243	26.0
Fe_2Cu_6	Fe	1.413	2.495	0.077	2.572	25.81
	Cu1	1.413	0.063	0.005	0.068	29.05
Fe_1Ag_5	Fe	1.597	3.011	0.117	3.128	25.99
	Ag1	1.597	0.025	0.002	0.027	27.99
hcp Co		1.384	1.602	0.087	1.689	27.0
Co_2Cu_6	Co	1.413	1.562	0.094	1.656	26.98
	Cu1	1.413	0.015	0.003	0.018	29.03
Co_2Pd_4	Co	1.429	1.885	0.136	2.021	26.97
	Pd1	1.535	0.287	0.032	0.319	45.99
	Pd2		0.272	0.032	0.304	46.04
Co_2Pt_4	Co	1.429	1.872	0.125	1.997	27.00
	Pt1	1.551	0.199	0.042	0.241	78.00
	Pt2		0.071	0.009	0.080	78.00

Table I. This is due to the fact there is almost no Cu (Ag) d states around the Fermi energy to hybridize with Fe (Co) d states. Consequently, magnetic interaction between the Fe (Co) monolayers and the neighboring Cu (Ag) layers is small. In contrast, the Pd (Pt) d band is not completely filled, and there is a significant number of Pd (Pt) d states near the Fermi level. Thus, the magnetic interaction between the Co monolayers and the neighboring Pd (Pt) layers are much stronger and, hence, much larger induced magnetic moments in the Pd (Pt) layers. Finally, Table I shows that there is little charge transfer between the Fe (Co) monolayers and the neighboring Cu (Pd, Ag, Pt) layers.

IV. CIRCULAR MAGNETIC X-RAY DICHROISM

X-ray absorption spectra were calculated from the spin-polarized relativistic band structures using the golden rule (see Sec. II). To obtain more accurate conduction bands, which are the final states in the x-ray absorption process, these band structures were obtained with the so-called combined correction terms included.[11] The initial core states were solutions to the fully relativistic, spin-polarized Dirac equation.[16]

The calculated x-ray absorption spectra for Fe and its Fe/Cu(Ag) multilayers, Co and its Co/Pd(Pt,Cu) multilayers, are plotted in Figs. 1 and 2, respectively. For comparison with experiments, we broadened the raw theoretical spectra (sharp curves) with Lorentzians to take into account core-hole lifetime effects, and also convoluted them with a Gaussian to simulate experimental resolution. The broadened spectra are also plotted in Figs. 1 and 2 (smooth curves).

We note, firstly, that the CMXD signal is large in all the systems considered. For example, in terms of peak height asymmetries, the CMXD varies from 20 to 60% (see Figs. 1 and 2). The CMXD signal is particularly strong in the Fe-Ag and Co-Pd(Pt) multilayers [Figs. 1(e), 1(f), 2(b), 2(d), 2(e), and 2(g)]. We also see significant changes when going from bulk Fe and Co to their multilayers. For example, the Fe L_2 and L_3 edges from the Fe multilayer now each splits into two peaks while the height of the Co (Fe) absorption and dichroism signal in the Co-Pd(Pt) (Fe-Ag) multilayers increases substantially (see raw theoretical spectra in Figs. 1 and 2). This latter finding is in agreement with experiments by Wu *et al.*[21] Nevertheless, these changes do not show up very clearly in the broadened spectra (smooth curves). For example, there is no splitting in the broadened Fe L_2 and L_3 edges in Fe_2Cu_4 (001). We find that all the broadened spectra look very similar to experimental ones (Fig. 2 in Ref. 21 for the Fe systems, and Fig. 1 in Ref. 21 for the Co systems).

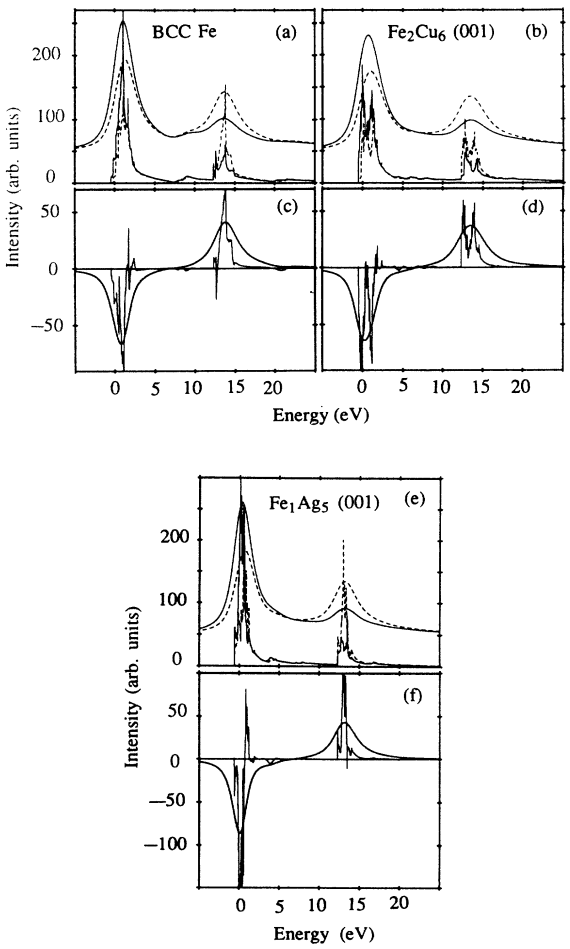

FIG. 1. Calculated x-ray absorption spectra: (a) bcc Fe, (b) Fe_2Cu_6 (001), and (e) $FeAg_5$ (001). Solid (dashed) curves are for left (right) circular x-ray polarization, μ^+ (μ^-). The corresponding circular magnetic dichroism ($\mu^+ - \mu^-$) is plotted in (c), (d), and (f), respectively. The smooth curves are the broadened raw theoretical spectra (sharp curves) by Lorentzians of width 1.4 eV (L_2) and 0.9 eV (L_3) and by a Gaussian [full width at half maximum (FWHM)=0.4 eV].

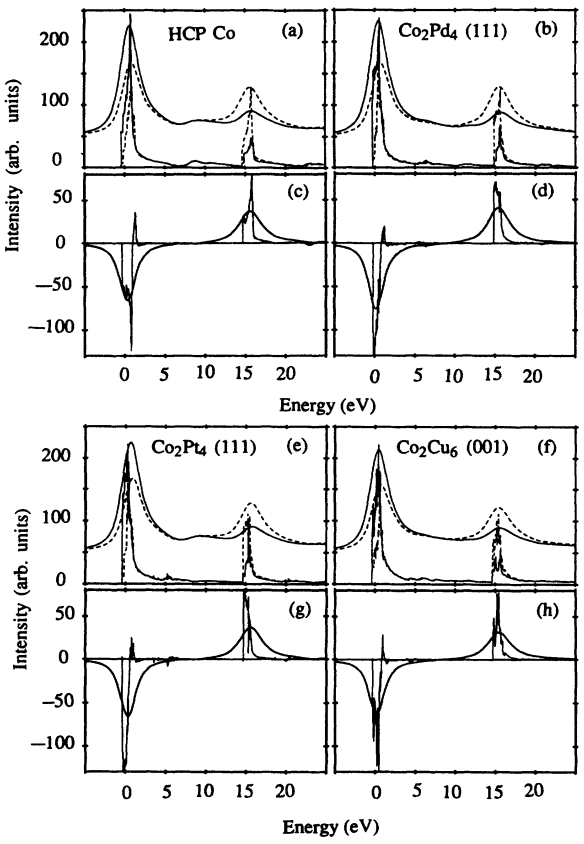

FIG. 2. Calculated x-ray absorption spectra: (a) hcp Co, (b) Co_2Pd_4 (111), (e) Co_2Pt_4 (111) and (f) Co_2Cu_6 (001). Solid (dashed) curves are for left (right) circular x-ray polarization, μ^+ (μ^-). The corresponding circular magnetic dichroism ($\mu^+ - \mu^-$) is plotted in (c), (d), (g), and (h), respectively. The smooth curves are the broadened raw theoretical spectra (sharp curves) by Lorentzians of width 1.3 eV (L_2) and 0.9 eV (L_3) and by a Gaussian (FWHM = 0.4 eV).

V. LINEAR MAGNETIC X-RAY DICHROISM

Linear MXD experiments may be classified into two types. One is to measure the difference in the x-ray absorption rate for two different magnetization directions with the photon polarization fixed. The other is to measure the difference in the x-ray absorption rate for two different photon polarizations with a fixed magnetization orientation. The first type is caused by the band-structure changes due to the rotation of the magnetization (i.e., magnetocrystalline anisotropy). In contrast, the second type is due to the different transition-matrix elements for two different photon polarizations. We want to point out that this second type also contains conventional linear dichroism due to single-site nonspherical potentials. Therefore, since in our present calculations only spherical potentials inside atomic spheres are included, our calculated LMXD spectra of the second type to be presented below, may be compared directly with experiments only for the systems where the single-site anisotropic potentials are small.

In an earlier paper,[23] we calculated x-ray absorption spectra for linear photon polarization as a function of

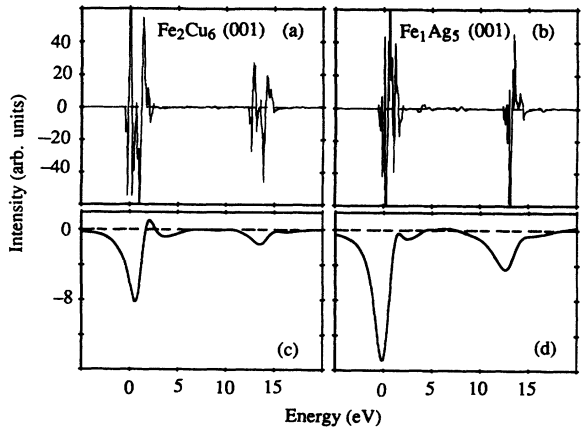

FIG. 3. Calculated linear dichroic x-ray absorption spectra $[\mu^x(\mathbf{m}\|\mathbf{z}) - \mu^z(\mathbf{m}\|\mathbf{z})]$: (a) Fe_2Cu_6 (001) and (b) $FeAg_5$ (001) multilayer. The smooth curves in (c) and (d), are the broadened raw theoretical spectra in (a) and (b) (see Fig. 1).

magnetization direction (LMXD of the first kind) for bcc Fe and its Fe_2Cu_6 multilayer and for hcp Co and its $Co_2Pd(Pt)_4$ multilayers $[\mu^x(\mathbf{m}\|\mathbf{z}) - \mu^x(\mathbf{m}\|\mathbf{x})]$. These LMXD spectra are very spiky and highly oscillatory. The oscillations perhaps reflect the small changes here and there in the band structure caused by the change of

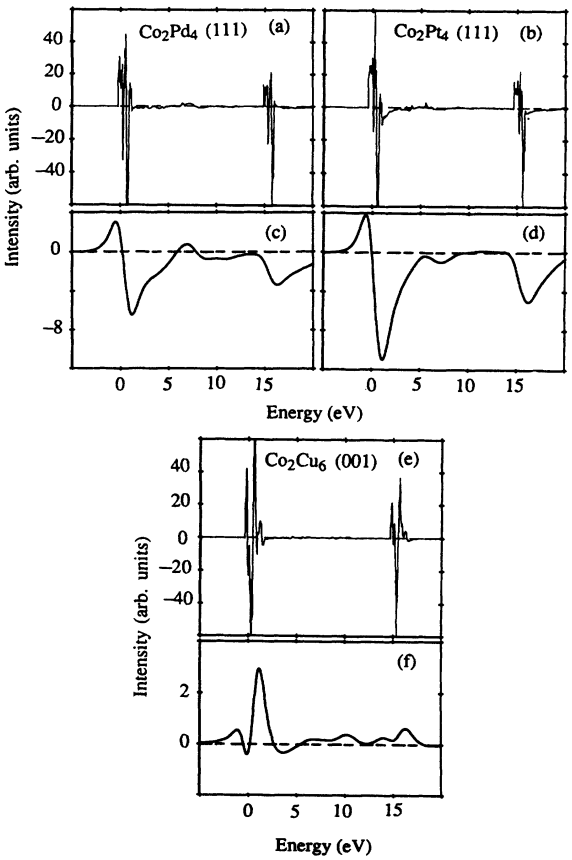

FIG. 4. Calculated linear dichroic x-ray absorption spectra $[\mu^x(\mathbf{m}\|\mathbf{z}) - \mu^z(\mathbf{m}\|\mathbf{z})]$: (a) Co_2Pd_4 (111), (b) Co_2Pt_4 (111) and (e) Co_2Cu_6 (001). The smooth curves in (c), (d), and (f) are the broadened raw theoretical spectra in (a), (b), and (f) (see Fig. 2).

the magnetization direction. The broadened spectra show some well defined shapes, but the amplitudes are tiny (within 1%). We have now also calculated LMXD spectra of the first kind for Fe in $FeAg_5$ (001) and for Co in Co_2Cu_6 (001). Again, the calculated LMXD spectra are very oscillatory. The broadened spectra are even smaller (within 0.5%) and thus, are not shown here. This smallness of the LMXD spectra perhaps explain why so far no experimental LMXD of this kind has been reported for bulk Fe and Co as well as their multilayers.

Here, we present calculated LMXD spectra of the second kind for Fe and Co multilayers. The calculated LMXD, defined as the difference in the absorption rate of x ray between photon polarization along x axis (100) and z axis (001) (grazing incidence) with magnetization parallel to z axis (001) $[\mu^x(\mathbf{m}\|\mathbf{z})-\mu^z(\mathbf{m}\|\mathbf{z})]$, is plotted in Figs. 3 and 4. We note that the raw theoretical LMXD spectra [Figs. 3(c), 3(b), 4(a), 4(b), and 4(c)] are also spiky and very oscillatory. Nevertheless, the broadened spectra [Figs. 3(c), 3(d), 4(c), 4(d), and 4(f)] show some simple features. These features are generally stronger (3–8%) than those in the LMXD spectra of the first kind. The features in the LMXD spectrum are similar between Fe_2Cu_6 (001) and $FeAg_5$ (001) [see Figs. 1(c) and 1(d)] and between Co_2Pd_4 (111) and Co_2Pt_4 (111) [see Figs. 2(c) and 2(d)].

VI. ORBITAL AND SPIN MAGNETIZATION SUM RULES

Thole *et al.*[4] and Altarelli[24] recently showed that in a localized ion model, the integral of the CMXD signal (I^o_{mxd}) over a given absorption edge is directly related to the local orbital magnetic moment ($\langle L_z \rangle$) by the following orbital magnetization sum rule:

$$\frac{I^o_{\mathrm{mxd}}}{I_t}=\frac{l(l+1)+2-c(c+1)}{2l(l+1)(4l+2-n)}\langle L_z\rangle \ , \tag{6.1}$$

where

$$I^o_{\mathrm{mxd}}=\int_{L_2+L_2} d\omega(\mu^+-\mu^-)$$

and

$$I_t=\int_{L_2+L_2} d\omega(\mu^++\mu^-+\mu^z) \ .$$

For $L_{2,3}$ edges, $c=1, l=2, n=n_d$ (occupation number of d states),

$$\frac{I^o_{\mathrm{mxd}}}{I_t}=\frac{\langle L_z\rangle}{2(10-n_d)}=\frac{\langle L_z\rangle}{2n_h} \ , \tag{6.2}$$

where n_h is the number of d holes. This sum rule suggests that CMXD is potentially a powerful probe of orbital magnetization since, as we have shown in Sec. IV, CMXD in most magnets is strong (i.e., easy to measure) and also it is element specific. Indeed, this sum rule has been used to derive the orbital magnetic moments from the measured CMXD for Ni,[4] Co and Co/Pd multilayers.[21] However, in an itinerant ferromagnet, the localized ion theory may not be generally applicable because of the interatomic hybridizations, and band theory may be a more appropriate description of the ground-state properties. The sum rule has not been derived from the band theory. Therefore, the validity and usefulness of this sum rule is not yet clear. In our earlier paper on this topic,[23] we checked this sum rule numerically in a straightforward manner using the results of our band theoretical calculations. We found that the sum rule holds only qualitatively. The orbital magnetic moment ($\langle L_z \rangle$), derived from the theoretical CMXD signal using the sum rule, is smaller than that calculated from the same band structure (m_o), by about 30–50%.

Interestingly, Eq. (6.2) indicates that if the sum rule holds [i.e., the integrated CMXD signal (I^o_{mxd}) is proportional to the orbital moment $\langle L_z \rangle$], the total absorption (I_t) should be proportional to the number of d holes n_h. Whereas the number of d holes (n_h) will be zero if the Fermi level is at the top of the d-band manifold, the total absorption (I_t) will not. This suggests that only those x-ray absorptions involving transitions into the empty d bands should be included in I_t. In our earlier paper,[22] to get the total absorption I_t, we integrated the x-ray-absorption spectra, blindly, over an energy range up to about 30 eV above the Fermi level where the photoexcitations from Fe (Co) $2p$ states exhaust completely. The total absorption I_t obtained in this way may be too large and consequently, the derived orbital magnetic moment too small. A more meaningful way of checking the validity of the sum rule is perhaps to impose an energy cutoff above the Fermi level. We note that the integrated CMXD signal I^o_{mxd} saturates at the energy of only a few eV above the Fermi level (or a few eV above the $L_{2(3)}$ edges). This can also be seen in Figs. 1 and 2. In Table II, we list the integrated CMXD signals (I^o_{mxd}) and total x-ray absorptions (I_t) as well as derived and theoretical

TABLE II. Integrated circular magnetic dichroism (I^o_{mxd}) (see text), integrated total absorption (I_t) (in the arbitrary unit), d-state occupation number (n_d), and orbital magnetic moments for Fe in bcc Fe, Fe_2Cu_6 (001), and $FeAg_5$ (001), and for Co in hcp Co, Co_2Cu_6 (001), and $Co_2Pd(Pt)_4$ (111). m_o denotes theoretical orbital magnetic moments and $\langle L_z \rangle$ orbital magnetic moment obtained using the orbital moment sum rule [Eq. (6.2)].

	System	I_{mxd}	I_{tot}	n_d	$\langle L_z\rangle$ (μ_B)	m_o (μ_B)
Fe in	bcc Fe	0.425	86.61	6.57	0.034	0.053
	Fe_2Cu_6	0.773	85.03	6.61	0.062	0.085
	Fe_2Cu_y[a]	0.685	85.29	6.61	0.054	0.076
	$FeAg_5$	1.166	83.09	6.69	0.093	0.123
	$FeAg_5$[a]	0.992	82.70	6.69	0.079	0.108
Co in	hcp Co	0.956	67.84	7.57	0.068	0.084
	Co_2Cu_6	1.092	67.24	7.66	0.076	0.093
	Co_2Cu_6[a]	1.187	67.31	7.66	0.082	0.101
	Co_2Pd_4	1.474	69.78	7.55	0.104	0.128
	Co_2Pd_4[a]	1.179	70.02	7.55	0.083	0.104
	Co_2Pt_4	1.253	72.27	7.55	0.083	0.110
	Co_2Pt_4[a]	0.755	71.86	7.55	0.051	0.071

[a]The magnetization of the system is in plane.

orbit magnetic moments ($\langle L_z \rangle$ and m_o) for bulk Fe and Co as well as their multilayers. The energy cutoff (E_{cut}) chosen is 10 eV for the Fe systems and 8 eV for the Co systems. We found that in both cases, the integrated CMXD signals are almost saturated at the cutoff energies. Note that theoretical magnetic moments (m_o in Table II and m_s in Table III) were calculated from the band structures with the combined correction terms included, and that they are slightly different from those obtained from the band structure without the combined correction terms (Table I). Table II shows that there is a better agreement between $\langle L_z \rangle$ and m_o than before.[23] Nevertheless, $\langle L_z \rangle$ is still about 30–35% smaller than m_o in some cases. One may say that the sum rule, at best, holds semiquantitatively. Interestingly, the anisotropy orbital moments in the multilayers are given rather accurately by the sum rule (see Table II). For example, the theoretical anisotropy moment $\Delta m_o^{001-100}$ is 0.009 (0.015) for Fe_2Cu_6 ($FeAg_5$), compared with the derived anisotropy moment $\Delta\langle L_z \rangle^{001-100}$ of 0.008 (0.014).

One may suggest that the sum rule (6.2) be applied only to the transitions to d states. Nevertheless, excluding transitions to Fe (Co) 4s states by setting the 2p-4s transition elements to zero, does not change the numbers listed in Table II significantly, and consequently does not improve the agreement between $\langle L_z \rangle$ and m_o. This also indicates that the x-ray absorptions are almost completely determined by the 2p-3d transitions.

Even if the sum rule does hold, it is perhaps still difficult to use it in practice because it is not easy to determine the cutoff energy for a magnet unambiguously in the measurements. Alternatively, if the integrated CMXD signal (I^o_{mxd}) is proportional to the orbital moment $\langle L_z \rangle$ for a particular magnetic ion, say, Fe or Co, for instance, one can determine the local orbital magnetic moment of the ion from the measured CMXD signals by fixing the universal constant for the ion before hand. We now explore this possibility. In Fig. 5, we compare $C_{atom} I^o_{mxd}$ with m_o. The scaling constant $C_{Fe(Co)} = m_o / I^o_{mxd}$ was calculated using results for an arbitrary system (Fe_2Cu_6 for Fe and Co_2Pd_4 for Co). Figure 5 demonstrates that for the systems under investigation at least, I^o_{mxd} is nearly proportional to m_o.

TABLE III. Integrated circular magnetic dichroism (I^s_{mxd}) (see text), integrated total absorption (I_t) (in the arbitrary unit), d-state occupation number (n_d) and spin magnetic moments for Fe in bcc Fe, Fe_2Cu_6 (001), and Fe_1Cu_5 (001), and for Co in hcp Co, Co_2Cu_6 (001) and $Co_2Pd(Pt)_4$ (111). m_s denotes theoretical spin magnetic moments and $\langle 2S_z \rangle$ spin magnetic moment obtained using the spin moment sum rule [Eq. (6.4)] (neglecting $\langle T_z \rangle$).

	System	I^s_{mxd}	I_{tot}	n_d	$\langle 2S_z \rangle$ (μ_B)	m_s (μ_B)
Fe in	bcc Fe	15.84	86.61	6.57	1.882	2.214
	Fe_2Cu_6	16.37	85.03	6.61	1.958	2.461
	Fe_2Cu_6[a]	20.25	85.29	6.61	2.415	2.461
	$FeAg_5$	17.53	83.09	6.69	2.095	2.944
	$FeAg_5$[a]	20.39	82.70	6.69	2.448	2.944
Co in	hcp Co	14.18	67.84	7.57	1.524	1.581
	Co_2Cu_6	13.04	67.24	7.66	1.361	1.501
	Co_2Cu_6[a]	12.81	67.31	7.66	1.334	1.502
	Co_2Pd_4	15.72	69.78	7.55	1.656	1.841
	Co_2Pd_4[a]	15.80	70.02	7.55	1.659	1.841
	Co_2Pt_4	15.78	72.27	7.55	1.605	1.849
	Co_2Pt_4[a]	15.77	71.86	7.55	1.613	1.850

[a]The magnetization of the system is in-plane.

Now we consider the recently proposed spin magnetization sum rule.[15] Carra *et al.* recently derived the following sum rule also in a localized ion model:

$$\frac{I^s_{mxd}}{I_t} = \frac{l(l+1)-2-c(c+1)}{3c(4l+2-n)}\langle S_z \rangle + \frac{l(l+1)[l(l+1)+2c(c+1)+4]-3(c-1)^2(c+2)^2}{6lc(l+1)(4l+2-n)}\langle T_z \rangle , \tag{6.3}$$

where $\langle S_z \rangle$ is the spin moment, T is an operator ($T = \sum_i \mathbf{s}_i - 3\mathbf{r}_i(\mathbf{r}_i \cdot \mathbf{s}_i)/r_i^2$) and

$$I^s_{mxd} = \int_{L_3} d\omega(\mu^+ - \mu^-) - \frac{c+1}{c}\int_{L_2} d\omega(\mu^+ - \mu^-) .$$

The authors suggested that this spin magnetization sum rule be used in determining the spin magnetic moments from the CMXD experiments on the systems where $\langle T_z \rangle$ is expected to be small. For $L_{2,3}$ edges, $c = 1, l = 2, n = n_d$,

$$\frac{I^s_{mxd}}{I_t} = \frac{1}{3n_h}\langle 2S_z \rangle + \frac{7}{6n_h}\langle 2T_z \rangle , \tag{6.4}$$

where

$$I^s_{mxd} = \int_{L_3} d\omega(\mu^+ - \mu^-) - 2\int_{L_2} d\omega(\mu^+ - \mu^-) .$$

We listed the integrated CMXD signals (I^s_{mxd}), total x-ray absorptions (I_t), and derived spin magnetic moments ($\langle 2S_z \rangle$) neglecting $\langle 2T_z \rangle$) using (6.4), together with theoretical spin magnetic moments (m_s) in Table III.

Table III indicates that for the Co systems, there is a rather good agreement between theoretical spin magnetic moments (m_s) and the spin magnetic moments derived from the sum rule ($\langle 2S_z \rangle$). $\langle 2S_z \rangle$ is generally about 10% smaller than m_s. For the Fe systems, however, the difference between the theoretical and derived spin magnetic moments varies from 2 to 30%. Importantly, the spin magnetic anisotropy for the Fe multilayers given by the sum rule is wrong. For instance, the theoretical spin magnetic anisotropy moment $\Delta m_s^{001-100}$ is zero for $FeAg_5$, compared with the derived one $\Delta\langle 2S_z \rangle^{001-100}$ of $0.353\mu_B$. This suggest that one should apply the spin magnetization sum rule (6.4) with caution to itinerant magnets.

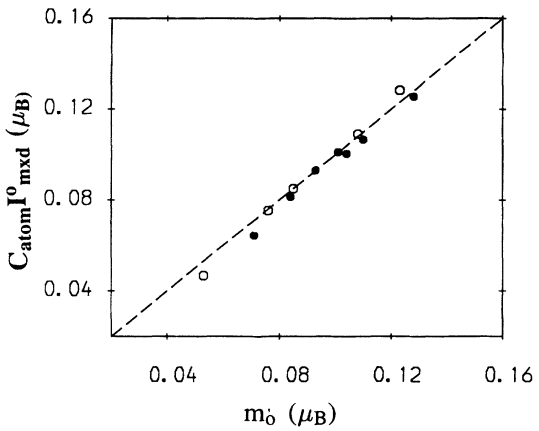

FIG. 5. The integrated CMXD signal ($C_{atom}I^{o}_{mxd}$) versus the orbital magnetic moment m_o. The scaling constant for Fe (Co atom, $C_{Fe(Co)}=m_o/I^{o}_{mxd}$ is determined using m_o and I^{o}_{mxd} for Fe_2Cu_6 (001) [Co_2Cu_6 (001)]. I^{o}_{mxd} and m_o are taken from Table II. Open circles are for the Fe systems and solid circles are for the Co systems.

VII. CONCLUSIONS

In this paper, we have described a fully relativistic spin-polarized band theory of polarized x-ray absorption by a magnetic solid. Both the initial core states and the final conduction bands are solutions to the spin-polarized Dirac equation, and the relativistic electron-photon interaction operator is used. Using this theory, we have calculated CMXD and LMXD spectra for bulk Fe and Co as well as their multilayers. We find that CMXD is large (20–60 %) in all the systems considered. In particular, as for the calculated orbital magnetic moments, the CMXD is enhanced when going from bulk Fe and Co to their multilayers. In contrast, we find that the LMXD due to the magnetocrystalline anisotropy, is perhaps too small (within 1%) to be measured. Nevertheless, the LMXD due to a change of photon polarization, say, from in-plane to normal-to-plane, is larger (3–8 %). We hope that this latter finding will encourage LMXD experiments on magnetic multilayers.

We have studied the recently proposed orbital and spin magnetization sum rules[4,15] in light of our band-theoretical results. We find that the orbital magnetization sum rule (6.2) holds, at best, semiquantitatively in the band theory. The orbital magnetic moments given by the sum rule are too small by 20–35 %. Furthermore, we believe it may be difficult to use in practice because it is perhaps not easy to determine the arbitrary energy cutoff unambiguously. Alternatively, we suggest that one can use a simple linear relationship between the integral of the CMXD and the orbital magnetic moment to measure the orbital magnetic moment. We also find that the spin magnetization sum rule (6.4) is a rather good approximation for bulk Co and its multilayers. However, the spin magnetization sum rule breaks down qualitatively for highly anisotropic systems such as Fe multilayers studied here.

[1]M. Blume, J. Appl. Phys. **57**, 3615 (1985); D. Gibbs, D. R. Harshman, E. D. Isaacs, D. B. McWhan, D. Mills, and C. Vettier, Phys. Rev. Lett. **61**, 1241 (1988); L. Baumgarten, C. M. Schneider, H. Petersen, F. Schäfers, and K. Kirschner, *ibid.* **65**, 492 (1990).

[2]G. Schütz, W. Wagner, W. Wilhelm, P. Kienle, R. Zeller, R. Frahm, and G. Materlik, Phys. Rev. Lett. **58**, 737 (1987); G. Schütz, M. Knülle, R. Wienke, W. Wilhelm, W. Wagner, P. Kienle, and R. Frahm, Z. Phys. B **73**, 67 (1988); R. Wienke, G. Schütz, and H. Ebert, J. Appl. Phys. **69**, 6147 (1991).

[3]B. T. Thole, G. van der Laan, and G. A. Sawatzky, Phys. Rev. Lett. **55**, 2086 (1985); G. van der Laan, B. T. Thole, G. A. Sawatzky, J. B. Goedkoop, J. C. Fuggle, J.-M. Esteva, R. Karnatak, J. P. Remeika, and H. A. Dabkowska, Phys. Rev. B **34**, 6529 (1986).

[4]B. T. Thole, P. Carra, F. Sette, and G. van der Laan, Phys. Rev. Lett. **68**, 1943 (1992).

[5]P. Kuiper, B. G. Searle, P. Rudolf, L. H. Tjeng, and C. T. Chen, Phys Rev. Lett. **70**, 1549 (1993).

[6]See, e.g., H. S. Bennett and E. A. Stern, Phys. Rev. **137**, A448 (1965).

[7]A. K. Rajagopal, J. Phys. C **11**, L943 (1978); A. H. MacDonald and S. H. Vosko, *ibid.* **17**, 3355 (1979).

[8]P. Strange, J. B. Staunton, and B. L. Gyorffy, J. Phys. C **17**, 3355 (1984).

[9]H. Ebert, P. Strange, and B. L. Gyorffy, J. Appl. Phys. **63**, 3055 (1988); H. Ebert and R. Zeller, Phys. Rev. B **42**, 2744 (1990).

[10]S. Stähler, G. Schütz, and H. Ebert, Phys. Rev. B **47**, 818 (1993).

[11]H. L. Skriver, *The LMTO Method* (Springer-Verlag, Berlin, 1984).

[12]H. Ebert, Phys. Rev. B **38**, 9391 (1988).

[13]G. Y Guo, W. M. Temmerman, and H. Ebert, Physica B **172**, 61 (1991).

[14]G. Y. Guo, W. M. Temmerman, and H. Ebert, J. Phys. Condens. Matter **3**, 8205 (1991); J. Magn. Magn. Mater. **104–107**, 1772 (1992).

[15]P. Carra, B. T. Thole, M. Altarelli, and X.-D. Wang, Phys. Rev. Lett. **70**, 694 (1993).

[16]H. Ebert, J. Phys Condens. Matter **1**, 9111 (1989).

[17]M. E. Rose, *Relativistic Electron Theory* (Wiley, New York, 1961).

[18]O. Jepsen and O. K. Andersen, Solid State Commun. **9**, 1763 (1971); G. Lehman and M. Taut, Phys. Status Solidi B **54**, 469 (1972).

[19]H. Ebert and G. Y. Guo, Solid State Commun. (to be published).

[20]J. G. Tobin, G. D. Waddill, and D. P. Pappas, Phys. Rev. Lett. **68**, 3642 (1992).

[21]Y. Wu, J. Stöhr, B. D. Hermsmeier, M. G. Samart, and D. Weller, Phys. Rev. Lett. **69**, 2307 (1992).

[22]U. von Barth and L. Hedin, J. Phys. C **5**, 1629 (1972).

[23]G. Y. Guo, H. Ebert, W. M. Temmerman, and P. J. Durham, in *Metallic Alloys: Experimental and Theoretical Perspectives,* edited by J. S. Faulkner and R. G. Jordan (Kluwer Academic, Dordrecht, 1994).

[24]M. Altarelli, Phys. Rev. B **47**, 597 (1993).